Measurement of aspheric mirror segments using Fizeau interferometry with CGH correction

James H. Burge†, Chunyu Zhao, and Matt Dubin
College of Optical Sciences, University of Arizona, Tucson, AZ 85721

ABSTRACT

Large aspheric primary mirrors are proposed that use hundreds segments that all must be aligned and phased to approximate the desired continuous mirror. We present a method of measuring these concave segments with a Fizeau interferometer where a spherical convex reference surface is held a few millimeters from the aspheric segment. The aspheric shape is accommodated by a small computer generated hologram (CGH). Different segments are measured by replacing the CGH. As a Fizeau test, nearly all of the optical elements and air spaces are common to both the measurement and reference wavefront, so the sensitivities are not tight. Also, since the reference surface of the test plate is common to all tests, this system achieves excellent control for the radius of curvature variation from one part to another. This paper describes the test system design and analysis for such a test, and presents data from a similar 1.4-m test performed at the University of Arizona.

Keywords: Optical testing, interferometer, computer generated holograms, astronomical optics

1. INTRODUCTION

Large telescope primary mirrors can be created from an array of smaller segments, such as the proposed Thirty Meter Telescope (TMT)[1] and the European Extremely Large Telescope (E-ELT)[2]. Both projects currently assume hexagonal mirror segments about 1.4 meters across. These telescopes will require hundreds of these segments, which have varying non-axisymmetric aspheric departure, and must match very closely in radius of curvature. The challenges of manufacturing, supporting, and controlling this large number of segments is daunting. We propose a measurement method that allows accurate and cost effective measurement of these mirror segments using Fizeau interferometry with computer generated holograms (CGHs). The designs here build on the heritage for the development of this test[3,4,5] incorporating significant changes in the detailed implantation, but the basic concept remains.

The test concept and preliminary design for E-ELT segments are provided in Sections 2 and 3. A comprehensive error analysis, including component errors and system alignment errors, is provided in Section 4, and Section 5 summarizes relevant hardware that has already been built at the University of Arizona.

2. INTRODUCTION TO FIZEAU MEASUREMENT WITH CGH

Clearly, there is a great advantage to measuring aspherical optics with a configuration that uses spherical references. There are also significant benefits in terms of cost and performance for Fizeau interferometry, which does not require accurate wavefront control. We propose to measure the off-axis segments using a Fizeau interferometer that has the following:

- Full aperture Fizeau test plate with spherical convex reference surface. Uses interference between reference and test wavefronts
  - Reference wavefront created from reflection of convex surface of test plate
  - Test wavefront from reflection from mirror segment
- Uses computer generated holograms to control the absolute and relative wavefronts
  - Common CGH, 60 mm diameter, corrects both reference and test wavefront.
  - Measurement CGH, 60 mm diameter, corrects only test wavefront (reference wavefront used at zero order). Both CGHs can be made as a single pattern on the same substrate

†J. H. Burge is Professor of Optical Sciences and Astronomy, University of Arizona. 520-621-8182, jburge@optics.arizona.edu

Modern Technologies in Space- and Ground-based Telescopes and Instrumentation, edited by Eli Atad-Ettedgui, Dietrich Lemke, Proc. of SPIE Vol. 7739, 773902 · © 2010 SPIE · CCC code: 0277-786X/10/$18 · doi: 10.1117/12.857816

- Phase shift interferometry, accomplished by pushing the test plate with PZTs, provides surface measurements. An alternate system that achieves simultaneous measurements of 4 frames with 90° phase shift using two polarization states has also been developed at the University of Arizona.
- Spinning ground glass diffuser or synthetic extended source to eliminate coherent noise
- Convex spherical surface calibrated *in situ* using a spherical reference mirror

The test configuration is shown below in Figure 1.

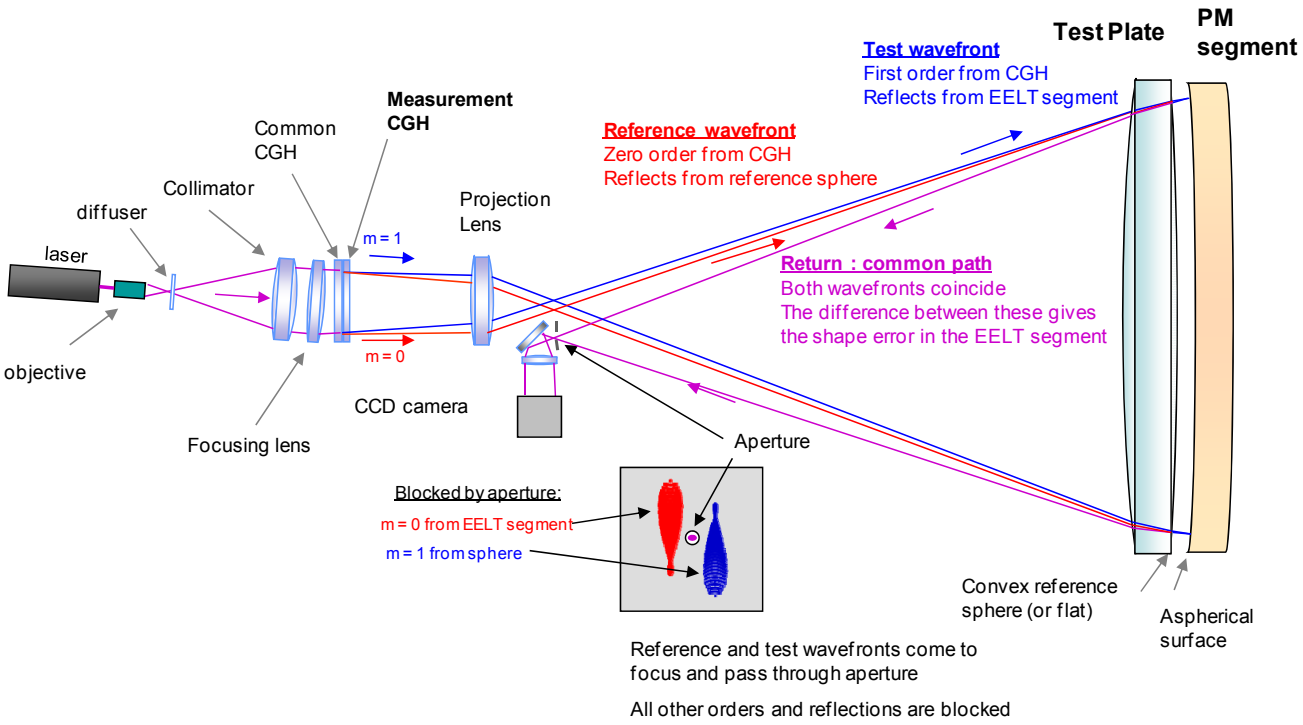

Figure 1. Schematic layout for the CGH Fizeau test. The test and reference wavefronts are split at the CGH (test wavefront uses +1 and reference wavefront uses 0 order of diffraction). They are recombined at the test plate so that they coincide for the imager.

Some advantages to this test are:

- Radius of curvature matching. The dominant error comes from the variation in the spacing between the test plate and the mirror segment. An uncertainty of 0.1 mm here causes only 1 nm rms error in the surface power.
- Efficient for measuring multiple segments. Once the system is aligned and calibrated, it is easy to reconfigure for measuring the various segment types. Only a single 60 mm CGH in a kinematic mount needs to be changed.
- Very low noise measurements using phase shift interferometry. To first order, all optics are common path, and affect the reference and test wavefronts the same. Vibration and atmospheric effects are limited to a 1-cm gap between the test plate and the mirror segment. The beams are not purely common path, with some shift, or shear, between the two wavefronts. This is treated below.
- Excellent imaging. The imaging system requires no wavefront correction, so the images are undistorted and can be made at very high spatial resolution. Furthermore, the diffuser in the projection portion of the system greatly reduces the coherent or speckle noise that often affects interferometric measurements.
- High accuracy. The measurements are not very sensitive to alignment errors, so the system can achieve accuracy of a few nm without requiring expensive mechanics. As both wavefronts coincide at the test plate, there is almost no measurement error due to surface irregularity on the back of the test plate or the test plate refractive index inhomogeneity.

An error in the surface being measured creates a deviation in the test wavefront that is measured directly with the interferometer. The wavefront error is precisely twice as large as the surface error that created it. For any single test, it is impossible to distinguish between an error in the mirror being measured and an error in the test plate itself. The wavefront error from a test plate irregularity is also exactly twice its figure error. For this reason, the test must be calibrated with a concave reference sphere, which is made to high accuracy. A different CGH is used to provide a null test for the sphere. The symmetry of the reference sphere can be used to calibrate the surface measurement. The reference sphere would be rotated and translated under the test. A maximum likelihood reconstruction can be used to separate the features that are fixed in the test from those that move with the reference sphere.[6]

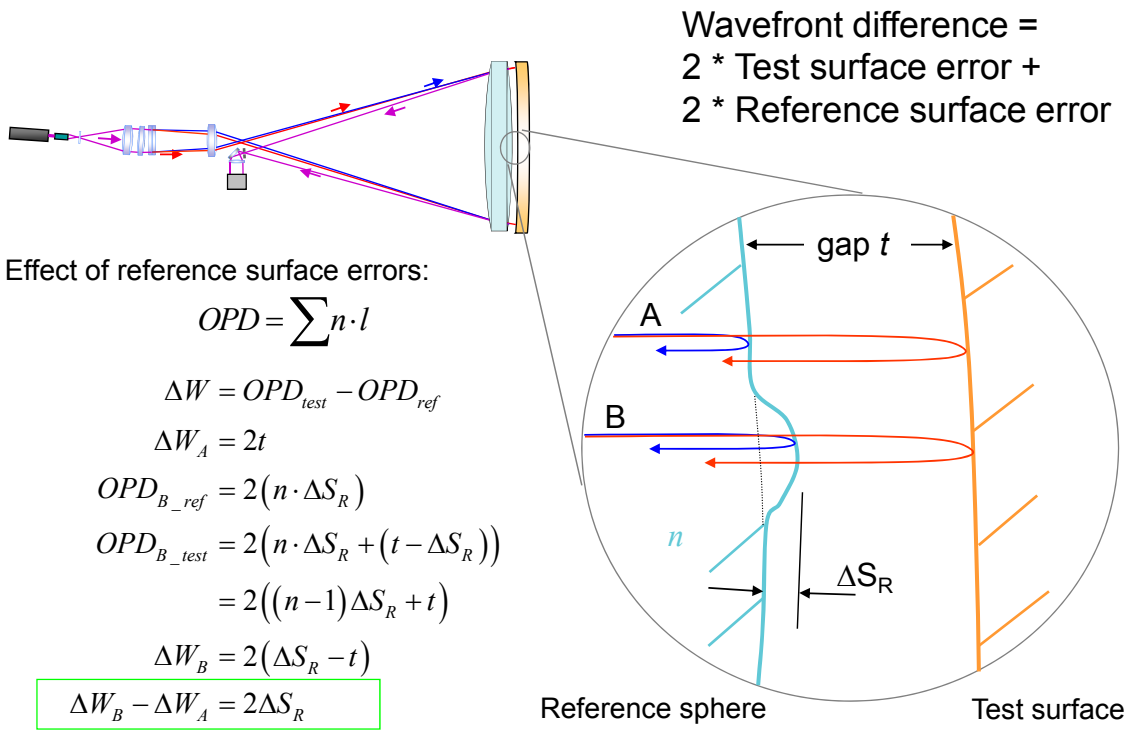

Figure 2. A "bump" in the reference surface of the test plate has exactly the same impact as a "bump" on the surface being measured. Both cause a bump in the wavefront which is twice as large as the surface feature.

The surface measurements are made using phase shift interferometry with the following features:

Phase shift interferometry

- The Fizeau interferometer provides a stable fringe pattern showing the difference in the two wavefronts
- Phase shift interferometry is used to capture this data
- The gap is varied to shift the interferogram by λ/4 increments. We do this by pushing the part with PZTs
- The interferograms are captured in a CCD camera and digitized
- The data from all frames are processed to provide a phase map
- Multiple maps are measured and averaged to reduce noise to < 1 nm rms
- UA has implemented simultaneous phase shifting version, including synthetic extended source to eliminate coherent noise,

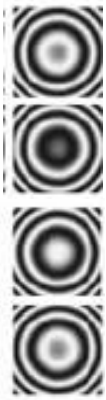

The nominal design of the optical test uses a point source created by a laser and objective lens. However, improved performance is achieved by replacing this with an extended source. As we require greater than 2 cm coherence length, we use a laser, making a simple extended source impossible. One way to achieve such a source is to project the laser light onto a spinning ground glass diffuser. Since the reference and test surfaces are nearly coincident, there is no significant degradation in contrast for the measurement. As long as the illuminated portion of the diffuser is aligned, symmetry preserves the accuracy.

3. DESIGN OF CGH FIZEAU TEST FOR E-ELT

The proposed European Extremely Large Telescope (E-ELT) requires a 42 meter primary mirror made from 984 hexagonal segments. The mean characteristics of the primary mirror are:

- Primary mirror radius of curvature: 84000 mm
- Primary mirror conic constant for the nominal radius of curvature : -0.9933
- Size of mirror segments: Nominally 1.23 m flat to flat, requiring test of 1.52 m diameter

3.1 Optical design of E-ELT test system

The optical design of the E-ELT system was developed in Zemax and optimized as a balance between performance and manufacturing difficulties. The nominal layout for the test is shown below.

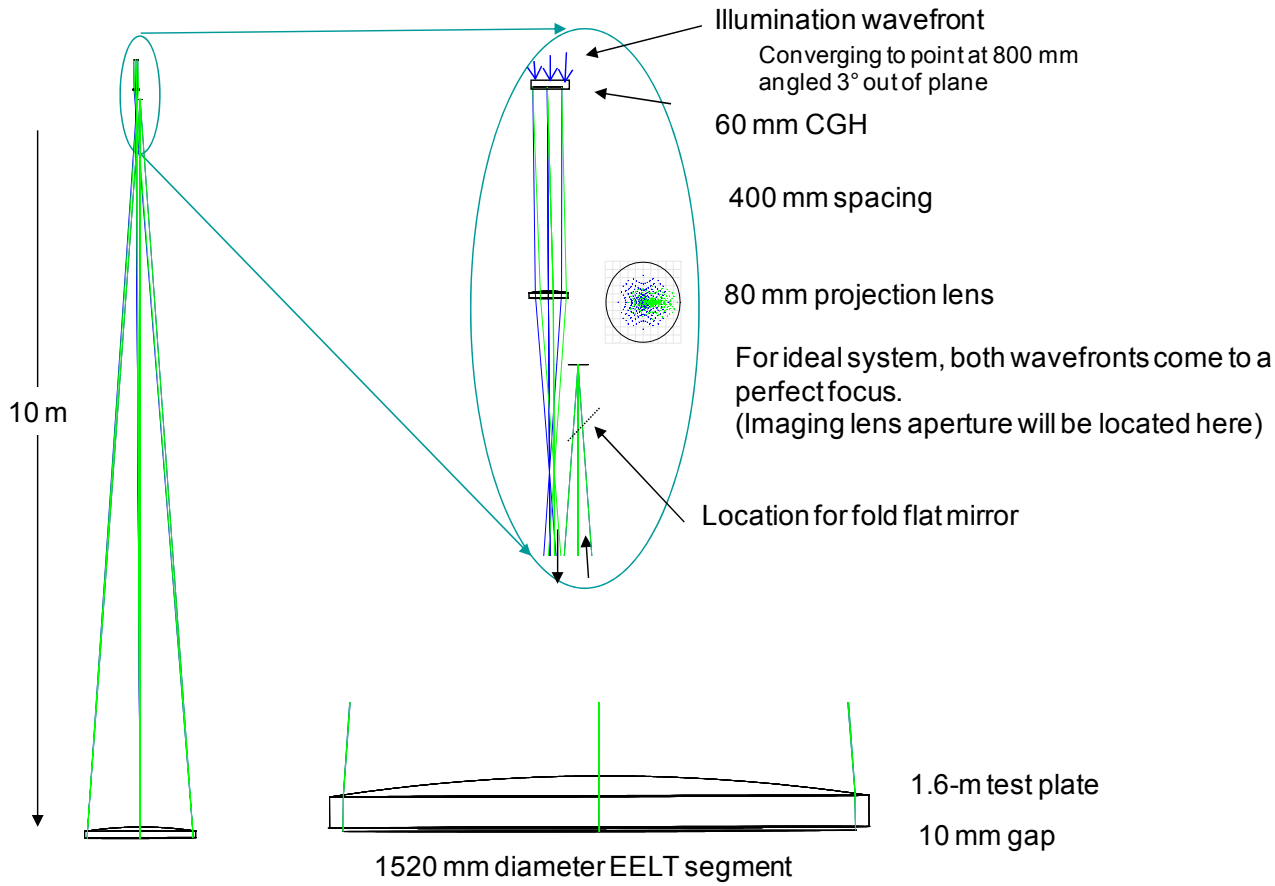

Figure 3. Layout of the Fizeau test for the E-ELT primary mirror segments.

The distance from the test plate to the intermediate focus was chosen as 10 meters as the result of a trade study that considered practical difficulties of manufacturing and alignment. In general, the tolerances get looser as the distance increases.

The holograms were designed to fit within 60 mm circular regions. We expect that these will be written onto 150 x 150 x 6 mm fused silica substrates. Each of the segment types and the reference sphere have their own CGH. We assume 4 patterns written per substrate. Kinematic mounting features are attached to allow positioning to < 10 µm in-plane (out of plane is better because mounts contact the glass itself). The CGHs also include alignment references that are used for locating the mirrors under test. The system will work with chrome on glass CGHs, but phase etched CGHs will eliminate possible ghost problem.

The preliminary designs of the CGH patterns are shown below in Figure 4. The CGH patterns are drawn as 1 line per 200 lines in the real part.

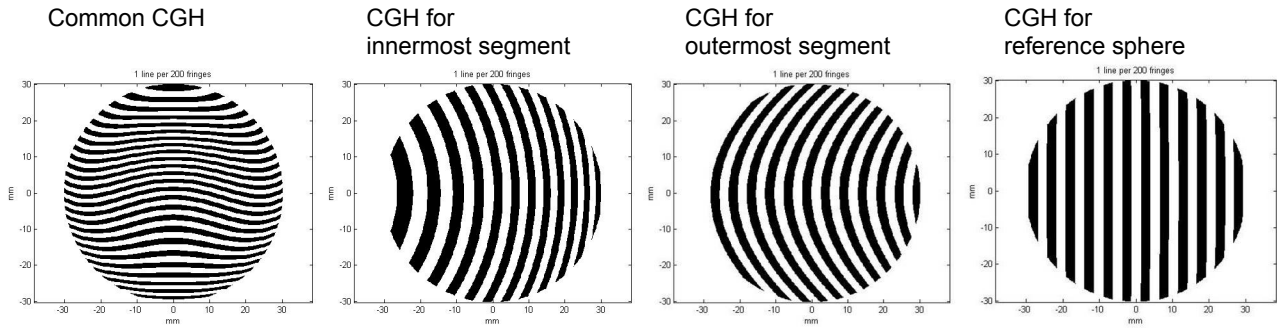

Figure 4. Pattern designs for the common CGH, which is the same for all segments, and measurement CGHs for the two extreme segments (innermost and outermost on the primary) and the reference sphere. The nominal line spacing is 12 µm for the common CGH and 26 µm for the measurement CGH. The patterns are plotted here with 200x synthetic wavelength, so each line here represents 200 lines in the real pattern.

The test was designed to allow complete isolation of the desired orders of diffraction. A plot of the different diffraction orders where the light comes to focus at an aperture is shown in Figure 5. The design presented here uses the 25 mrad slope between orders for the measurement CGH and 53 mrad for the common CGH. This carrier provides a region where the desired orders come to focus without any risk of pollution from the other light.

The laser and optics, CGH, projection lens, and imaging system will be built as a single assembly we call the BLISS (Beam launch and imaging sub-system design). This sub-system can be built and tested on its own, then interfaced with the test plate in a simple way. The layout of the BLISS system is shown below in Figure 6.

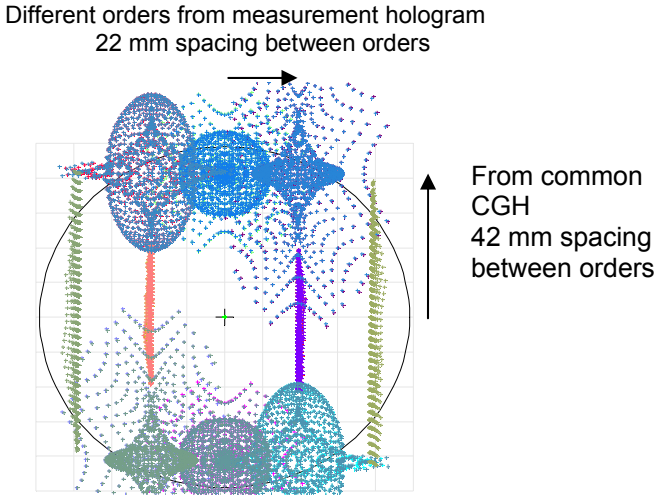

Figure 5. Distribution of the various orders of diffraction at the stop where the two desired orders of diffraction come to a sharp focus.

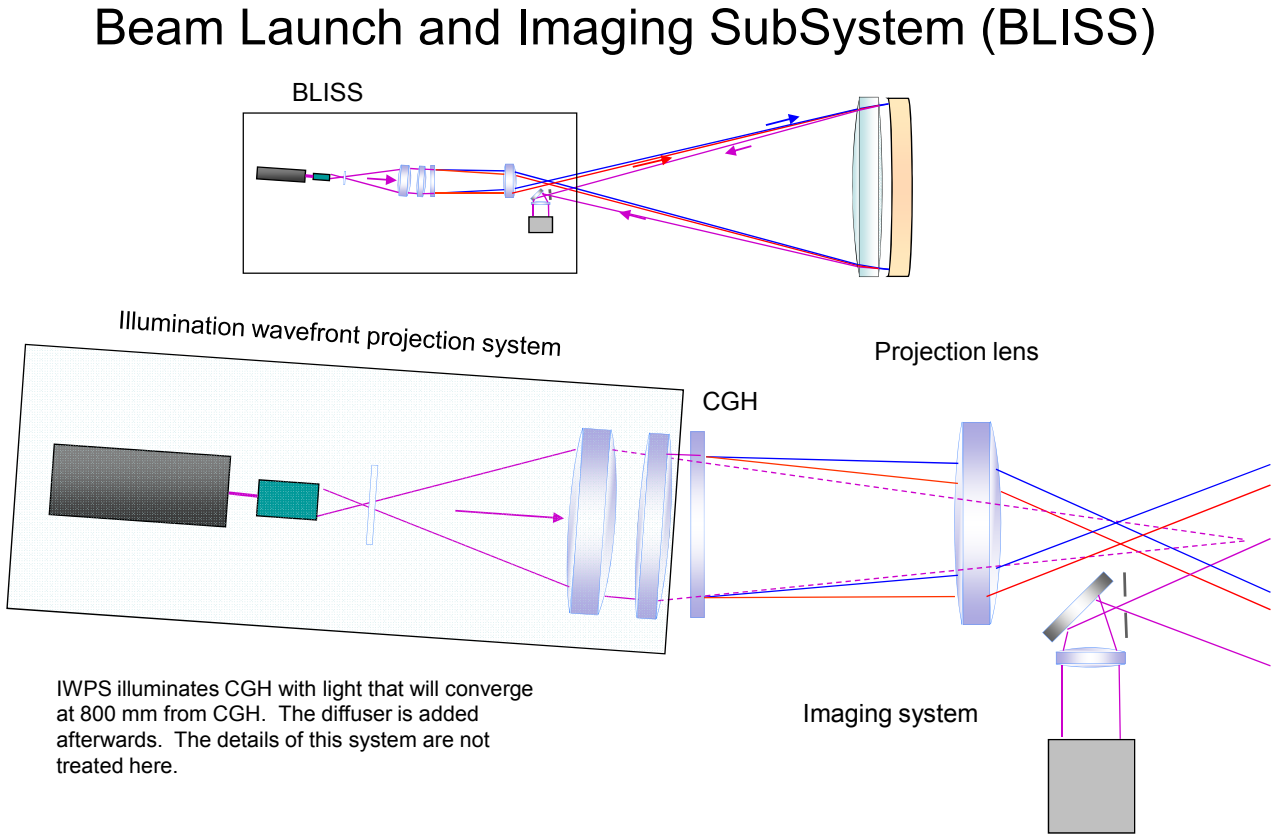

Figure 6. Conceptual layout of the Beam Launch and Imaging Subsystem

A simple, yet effective imaging system was designed, and is shown in Figure 7. This uses a single optical element to create a good image of the E-ELT segment onto a CCD, providing image size of 6 mm for the 1520 mm measurement diameter. The optical system was designed to accommodate a 5 mm aperture. This allows wavefront slope variations from the test plate up to ±0.25 mrad. The performance of the imaging system was shown to have real resolution of 750 pixels across the diameter, or about 2.0 mm resolution on the mirror under test. This system achieves excellent dynamic range. Assuming actual sampling of 500 pixels/diameter and 4 pixels/fringe, the system can measure fringe density up to 125 fringes/diameter, equivalent to +/- 26 µrad surface slope.

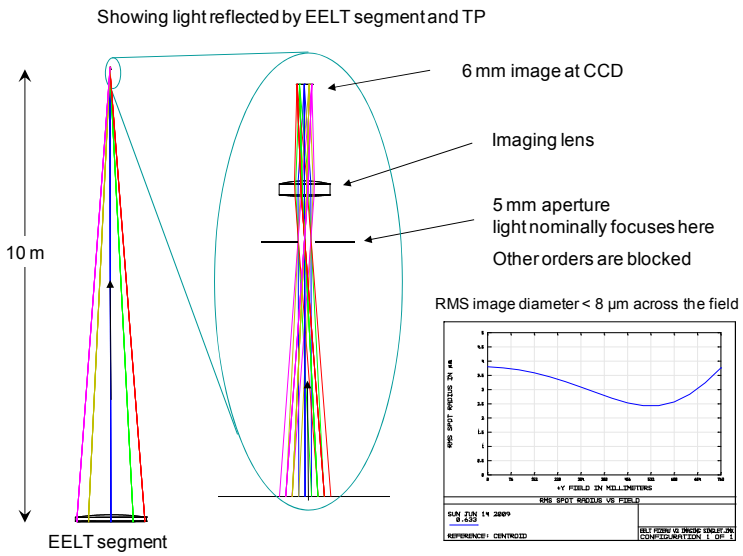

Figure 7. A simple imaging system isolates the desired orders of diffraction and provides 8 µm rms diameter point spread function across the 6 mm image, allowing real sampled information of 750 pixels across the mirror

3.2 Alignment procedure

The alignment procedure for this system builds on the experience at University of Arizona for similar systems. The steps for alignment are provided here:

1. Align BLISS (Beam launch and imaging sub-system)
    - Create Illumination wavefront
    - Align CGH to illumination wavefront using alignment telescope
    - Align projection lens to CGH using alignment telescope + mechanical measurements
    - Set location of CCD imaging system using mechanical measurements
2. Locate test plate with respect to BLISS
    - Use optical references projected from CGH + mechanical measurement
    - Tilt to return the reference wavefront into the imaging system
3. Align EELT segment to the test
    - Use references projected from CGH + mechanical measurement of gap for location
    - Coarse tilt to return the test wavefront into the imaging system
    - Fine tilt to null the fringes

The CGH provides optical references that are used to guide alignment. In particular, we use four different alignment patterns:

- Each CGH contains patterns that will create a set of images near the test plate through the projection lens. The locations of these images are used to set the position of the test plate and the EELT segment.
- The CGHs are kinematically mounted so they can be replaced with < 10 μm in plane and 5 μm out of plane repeatability. CGH patterns are used to define the positions of the mounting references to << 10 μm.

Each CGH has small unresolved features (< 50 um in size) that can be located for QC checks for the BLISS.

- An alignment CGH will be included that uses the same kinematic mounting, yet creates references for aligning the BLISS.

The test plate is aligned to the BLISS using a combination of optical references from the BLISS, mechanical measurements, and using the reflected light back into the BLISS. Each CGH has reference patterns written onto it which are imaged by the projection lens. The locations of these images can be located to < 0.1 mm using CCD cameras mounted to the test plate at appropriate locations. This concept and some images from other similar projects are shown in Figure 8. The 10 meter distance from the projection lens to the test plate can be set to 0.2 mm accuracy, using a laser tracker. The tilt of the test plate is adjusted to get the reflection from the reference surface into the imaging aperture.

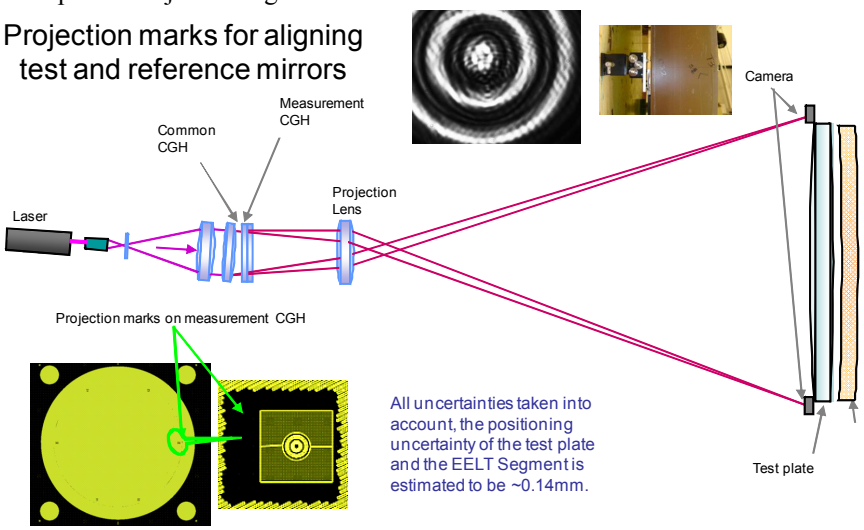

Figure 8. Reference marks on the CGH are imaged through the projection lens and are used to define alignment of the test plate and the mirror segments.

4. SUMMARY OF ERROR FOR CGH FIZEAU TEST OF E-ELT SEGMENTS

A comprehensive analysis was performed to allow an accurate assessment of the errors in the CGH Fizeau test. The following sources of error were considered:

- System alignment
  - Illumination wavefront quality
  - CGH
  - Projection lens
  - Test plate alignment
  - EELT segment alignment
- Fabrication errors of the components – coupled with beam shear (slight relative shift of two wavefronts)
- Errors from calibration with the reference sphere
- Residual from noise and spurious reflections

4.1 Direct simulation of errors

Many of the sources of error can be modeled and studied directly using lens design software. A complete perturbation analysis was performed to determine the coupling of assembly errors to surface measurement errors. This analysis was performed for the most extreme outside E-ELT segment. The analysis fully simulated the calibration of the system with the reference sphere.

The illumination wavefront was analyzed with 10 arcsec tilt, 2 waves of power, and a 0.25 wave rms with each of the low order Zernike terms. (The effects of these large wavefront errors was shown to be insignificant.) The CGH position errors were modeled as 25 μm lateral and tilt, 10 μm axial with a random change from measurement to measurement which is 20% as large. Errors in the projection lens include standard tolerances for the lens itself and 25 μm position error and 5 μm stability. Additional errors of about 20 nm rms in the projection lens transmitted wavefront, as represented by the lowest 35 Zernikes, are included. The test plate position is modeled as uncertain by 200 μm laterally and axially, and that the combination of the rear surface and the glass variations cause 7.5 waves rms, distributed as low order Zernikes. The position of the segment itself in the test introduces significant uncertainty. The tolerances for the mirror segment are:

140 μm radial position (shift in direction of parent axis)
5 mdeg clocking = 140μm/1.6m
100 μm axial position for 10 mm gap

The combined effect of all simulated errors is tabulated here. The details for each source of error are provided below. The dominant source of power (Z4) comes from the projection lens alignment. The dominant sources of astigmatism (Z5, Z6) come from the CGH and E-ELT alignment. The amounts of coma (Z7, Z8) and trefoil (Z9, Z10) are small. The projection lens provides most of the higher order residual, which is defined as all terms higher than Z10.

Table 1. Contributions to segment surface measurement errors. Units for Zernike coefficients are nm rms surface

Surface measurement error	Illum WF	CGHs	Projection Lens	TP	EELT	**RSS**
z4	0.4	1.4	3.4	2.0	1.3	**4.4**
z5	0.8	5.6	0.6	0.7	6.9	**8.9**
z6	0.2	1.4	4.0	2.1	0.5	**4.8**
z7	0.4	0.3	0.8	1.2	0.0	**1.5**
z8	0.2	1.3	0.8	0.7	0.1	**1.7**
z9	0.1	0.3	0.3	0.6	0.0	**0.7**
z10	0.1	1.1	0.3	0.9	0.0	**1.5**
residual	0.4	1.3	2.5	1.6	0.1	**3.2**
Total RSS	**1.1**	**6.3**	**6.0**	**3.8**	**7.0**	**11.9**

Aberration	**nm rms**
Power	4.4
Astigmatism	10.1
Coma	2.3
Trefoil	1.7
Residual	3.2
Total RSS	**11.9**

4.2 Statistical errors, evaluated by calculations rather than simulation

A number of effects are well understood, but do not lend themselves to modeling because they are more statistical in nature. These are treated below:

- Measurement CGH
  - Encoding error plus writing errors contribute **~1nm** rms error in wavefront
- Shear effects for illumination wavefront, CGH, test plate
  - The shear is small, couple the slope errors with shear
  - Conservative assessments are used here
    - 25 nm/cm rms wavefront slope
    - 10 nm/cm rms wavefront slope from CGH substrate
    - 100 nm/cm rms wavefront slope from test plate
  - This can be validated by moving the optics and measuring the change
- Shear effects for projection lens
  - The shear is large. Low order errors are already modeled. Look at errors that are uncorrelated over the 11 mm shear
  - 2 nm rms surfaces for scales < 11 mm
  - Assume uncorrelated for two surfaces 1.4 nm rms wavefront
  - Reference beam is same for calibration
  - Assume test beam shifts so it is uncorrelated (any correlation will improve the results)
  - This gives 2 nm rms wavefront
  - This can be validated by rotating the lens and measuring the change

The CGH Fizeau test uses different orders of diffraction from the measurement CGH, which depart the CGH at different angles. The projection lens brings the reference and test beams back together at the test plate. The angle between the beams is compensated by tilt between the reference surface and the mirror under test. The beams travel together from the reference surface to the CCD. The two wavefronts that will interfere do not coincide everywhere, in fact there can be significant lateral shift or shear between the beams, especially at the projection lens. The effect of shear on the measurements is due to the different coupling of irregularities to the two wavefronts. The effect depends on the shear magnitude and the slope and correlation length of the irregularities. The mean shear at the projection lens is 11 m, while the shear on the back of the test plate is only 0.06 mm.

Table 2. Contributions to wavefront errors from surfaces. Units are nm rms wavefront.

nm rms	Source of wavefront error
1.4	CGH encoding, EELT **and** calibration 1 nm x 1.414
0.5	Illumination WF 25 nm/cm, 200 um shear
0.3	CGH substrates 10 nm/cm, 200 um shear x 1.414
0.6	Test plate WF effect 100 nm/cm, 60 um shear
1.4	Projection lens calibration wavefront: rms wavefront variation over scales < 10 mm
1.4	Projection lens EELT wavefront: rms wavefront variation over scales < 10 mm
2.6	**RSS WF**

The distribution of such errors is not known. We take a conservative approach and assume 1.3 nm rms for higher order residual surface measurement errors **and** additional 1.3 nm rms taken as low order errors, with equal contributions into the low order terms.

4.3 Errors in calibration using the reference sphere

The use of the reference sphere is critical for the operation of this test. However, the use of this data introduces additional sources of error, analyzed as below:

- We assume a direct *in situ* calibration of the reference wavefront, as created from reflection from the convex reference surface on the test plate. The imaging is identical for this as for the E-ELT, but a different CGH is used.
- The calibration sphere is made slightly oversized (1.8-m). This allows this part to be translated and rotated, allowing separation of errors from Fizeau test and calibration sphere.
- Limitations:
  - Variations in calibration sphere figure for measurements 3 nm rms astigmatism, 2 nm rms additional low order
  - Uncorrelated changes in test plate figure after calibration : 3 nm rms astigmatism, 2 nm rms additional low order
  - Residual from noise: 1 nm rms residual

4.4 Residual from noise and spurious reflections

The effects of noise can be assessed by measuring repeatability and may be mitigated by averaging multiple measurements. We treat noise as follows:

- Experience has shown 3 – 10 nm rms per map. In practice, we average enough measurements to reduce the effect to < 1 nm rms.
- Here we budget residual of 1 nm rms for each low order Zernike term in addition to the residual.
- In addition, ghost fringes can cause 2 nm rms residual, but this can be mitigated with appropriate designs

4.5 Overall accuracy for Fizeau test

Combining all of the effects above predicts performance of 14.4 nm rms surface. Almost all of this is power and astigmatism. Afer removing these terms, the measurement errors are only 6.4 nm rms.

Table 3. Roll up of all error sources for the Fizeau test. Units are nm rms, surface.

	Alignment	Component residual	Calibration	Noise	RSS
	nm rms surface				
Power	4.4	0.6	2.3	1.0	5.1
Astigmatism	10.1	0.6	6.0	1.4	11.9
Coma	2.3	0.6	2.3	1.4	3.6
Trefoil	1.7	0.6	2.3	1.4	3.2
Residual	3.2	1.3	1.0	2.2	4.2
RSS	11.8	1.8	7.3	3.4	14.4
Specification					

Notes:

- The power error relates to the matching of the segments, The absolute radius is controlled to ~50 mm by measuring the sag of the calibration sphere to 2 μm
- The residual is proportionally more low frequency than small scale.

5. SYSTEM BUILT AT THE UNIVERSITY OF ARIZONA

A system very similar to that proposed here was already built at the University of Arizona. But in this case, the optical surface under measurement was the convex aspheric surface of a solid glass mandrel.[7] The convex surface, which is an off-axis paraboloid (OAP) was measured as shown below by looking through the blank and comparing the reflection from the asphere with light that is transmitted through the blank and reflected off a concave reference sphere.

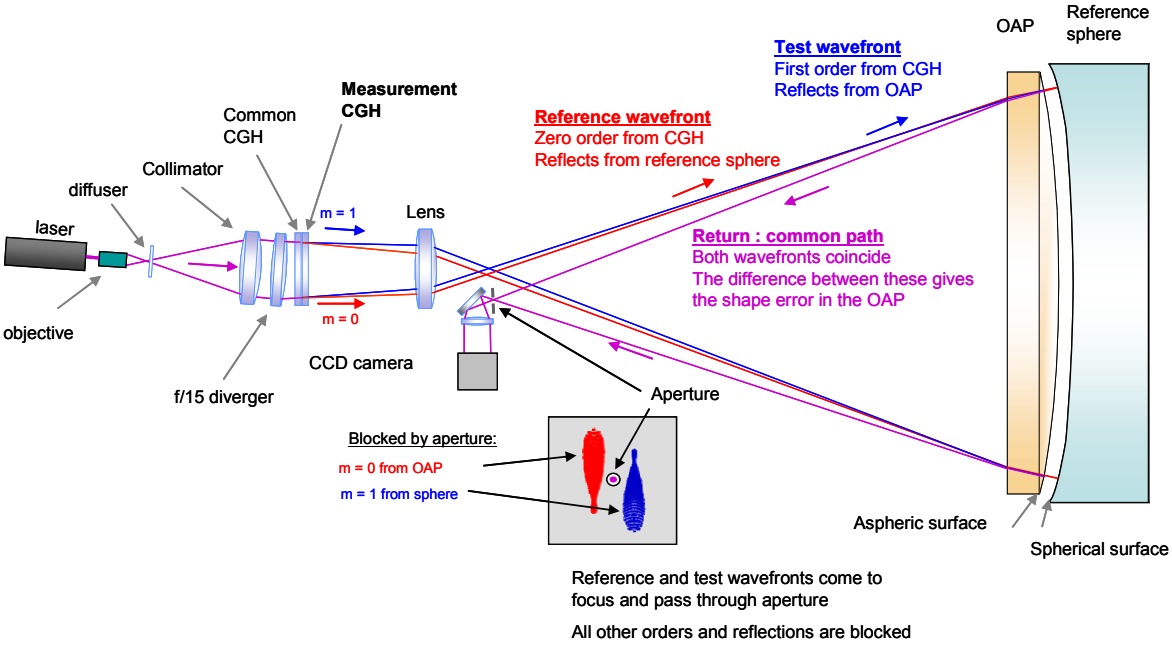

Figure 9. The layout for the mandrel tests is virtually identical to that for the segment measurements, except in this case the mandrel replaces the test plate, and is used in transmission so the convex aspheric surface is compared with a concave reference sphere.

BLISS optics on rail before installation in test tower

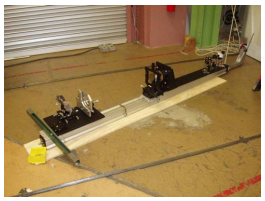

Looking up in the test tower, the BLISS and OAP are visible

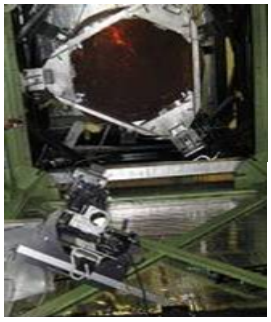

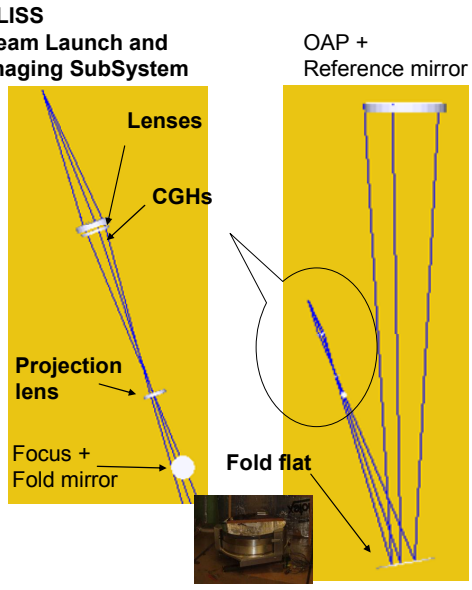

Figure 10. The optical layout of the test is show to scale, including the Beam Launch and Imaging SubSystem BLISS that points down to a fold flat and the OAP and reference sphere located at the top of the test tower.

One complication for this test is the requirement to view through the OAP substrate from below. This required the hardware to be mounted in the top of our 8-m test tower and for the beam train to be folded with a flat mirror. Figure 11 below shows much of the mechanical hardware, and Figure 12 shows the assembly sequence.

The load path that constrains the reference sphere with respect to the OAP was carefully designed to allow robust measurements in our noisy shop environment without isolation. The reference sphere is supported with vacuum, but constrained in position with hardpoints instrumented with load cells. The hardpoints are rigidly connected to the OAP support frame. Coarse adjustments are provided at this interface. Fine control for position and tilt of the OAP uses PZT actuators under the three support points. These are also used for phase shifting. The entire OAP frame/reference sphere combination is positioned with jackscrews.

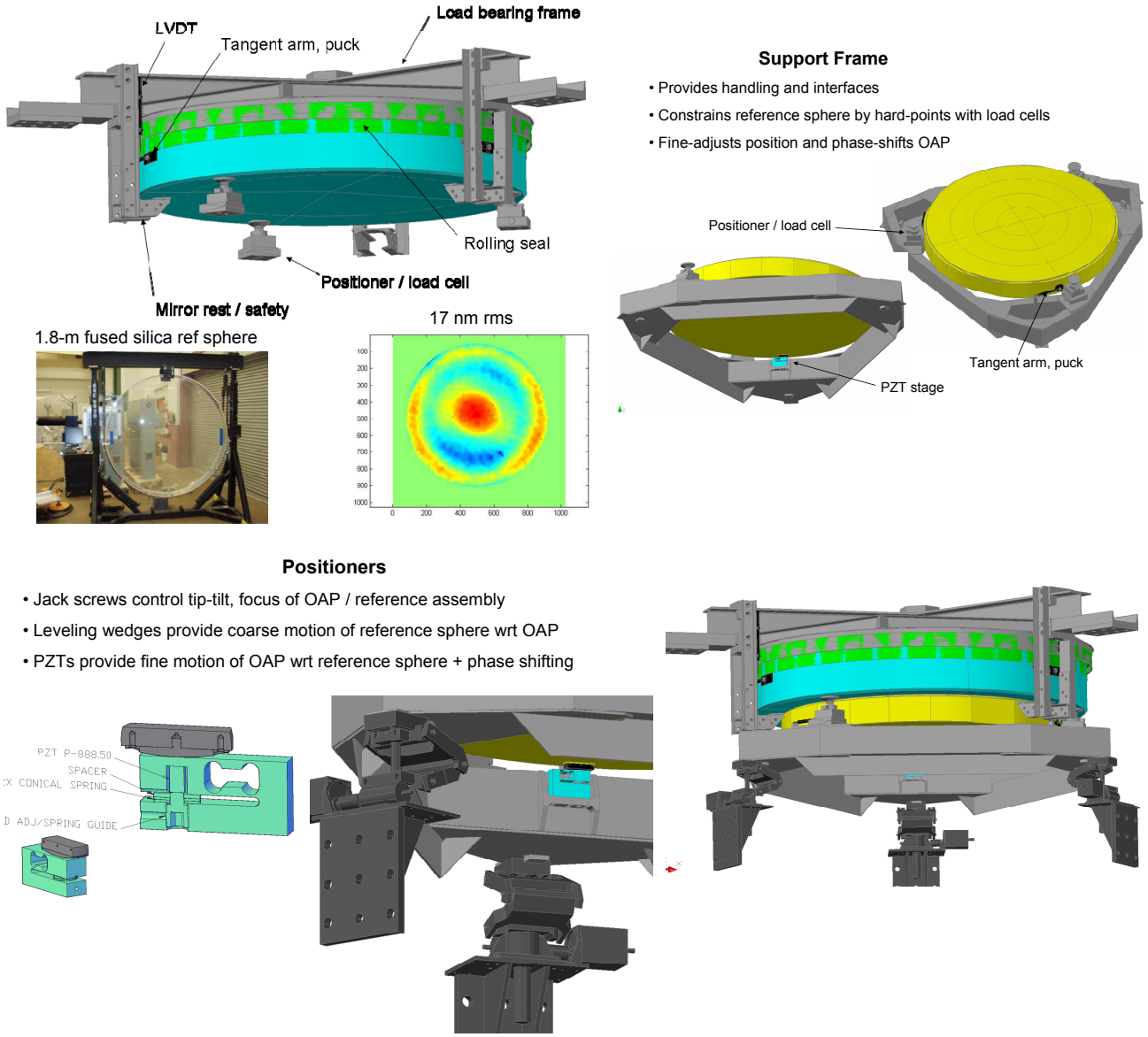

Figure 11. The hardware used to support the 1.8-m diameter fused silica reference sphere and the OAP allowed efficient installation of the OAP, motion control of the OAP-Reference sphere combination and control of the OAP with respect to the reference sphere. The reference sphere itself is supported with vacuum, yet is constrained in position with 3 hardpoints coupled closely to the OAP support.

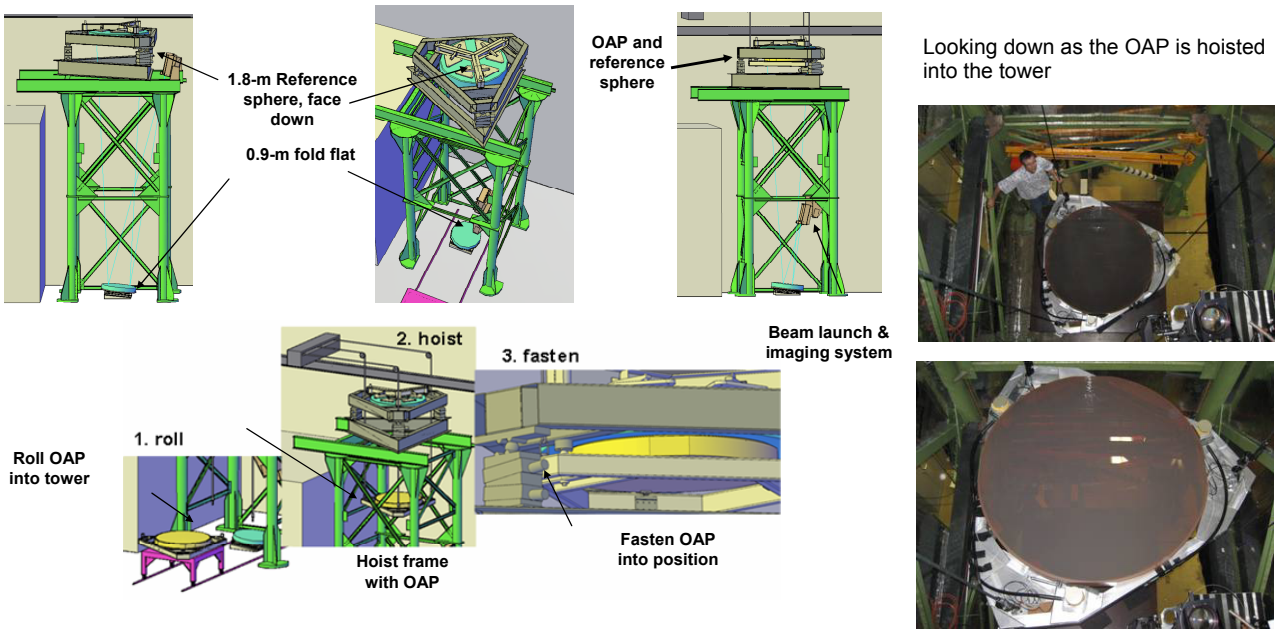

Figure 12. The OAP on its frame is loaded into the tower with a roll cart, then hoisted into position with 3 cables. Then it is rotated and captured with the main support hardware.

Two computer generated holograms were used. Both CGHs were laser-written onto 150 x 150 x 6 mm fused silica windows. The common CGH is fully common path, shared by both wavefronts. This pattern was phase etched into the surface. The measurement CGH defines the two wavefronts – the zero order light provides the reference and the first order diffraction provides the test wavefront. This pattern was made of chrome with 50% duty cycle.

The system provides accurate, low noise measurements as seen in Figure 13. Excellent fringe contrast was available. There were two interesting problems with the system. The solid state laser used had a small side lobe that would vary with time. This was measured with a spectrum analyzer and mitigated by carefully tuning an edge-pass filter. We also had two sets of ghost fringes that affected the data. One set, due to reflection between the holograms was easily corrected with alignment. A second set, which is a multiple reflection inside the hologram substrate remained throughout the test, causing background noise of ~1.5 nm rms.

Most errors in the phase shift interferometry system were eliminated by adding a slowly varying bias to the phase shift used for the measurements. This insures that the different maps in the average are taken at different bias phase. As long as the bias averages to zero, the effect of most types of error, such as phase shift error, detector nonlinearity, etc., will average to zero. Equivalently, many errors cause a phase measurement that "prints through" the fringe pattern into the phase data. If we shift the fringe pattern between measurements, then these types of errors average out.

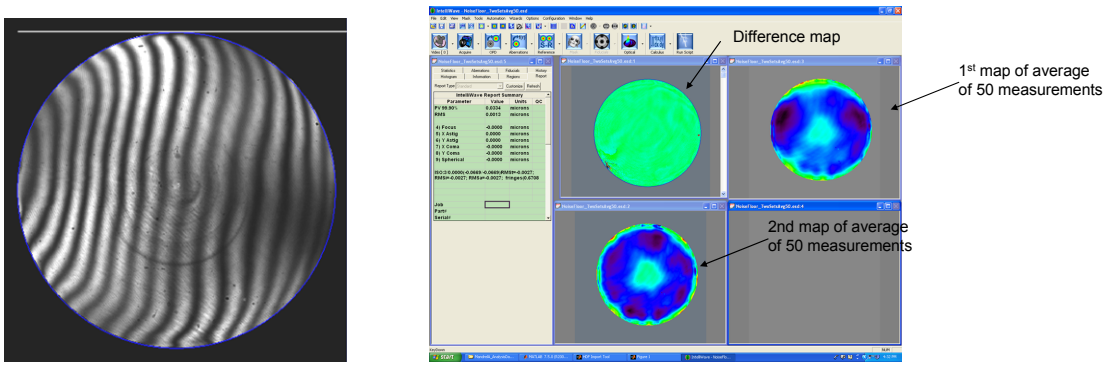

Figure 13. The Fizeau system provides excellent contract, low noise measurements. The repeatability of a single measurement, which consists of an average of 50 maps, shows only 1.3 nm rms.

This test is potentially sensitive to straie in the OAP substrates, which are small scale refractive index irregularities. The optical test uses two wavefronts that are not purely coincident in this region. There is up to 100 µm shear, or lateral shift, of the reference wavefront with respect to the test wavefront as the two go through the glass. This small difference is of no consequence for normal, low order variation in surface figure of refractive index. Although we could observe the effect of straie in the light system by defocusing or cutting the focused image with a knife edge, we could never find any measurement artifacts that correlated with the straie. Data shown below in Figure 14.

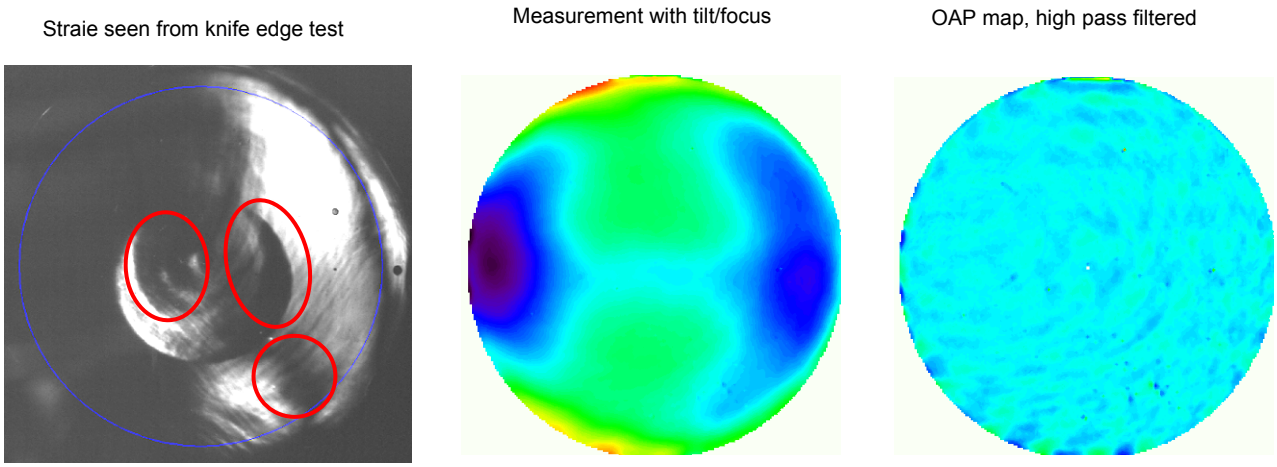

Figure 14. Although straie were visible in the OAP glass substrates, there was no discernable effect in the measurements. This image shows an interferogram with the straie clearly visible as gaps in the data from a knife edge test. When the knife is removed and the surface is measured, we can find no features in the data correlated with the straie. The residual features are around 1 nm rms, so we conclude that this effect must be < 1 nm rms for the OAP measurements.

The data from the Fizeau system matches nearly perfectly with that from an independent measurement with a swingarm optical CMM (SOC) shown in Figure 15. The primary differences are due to uncalibrated errors in the SOC and noise from the ghost fringes in the Fizeau test.

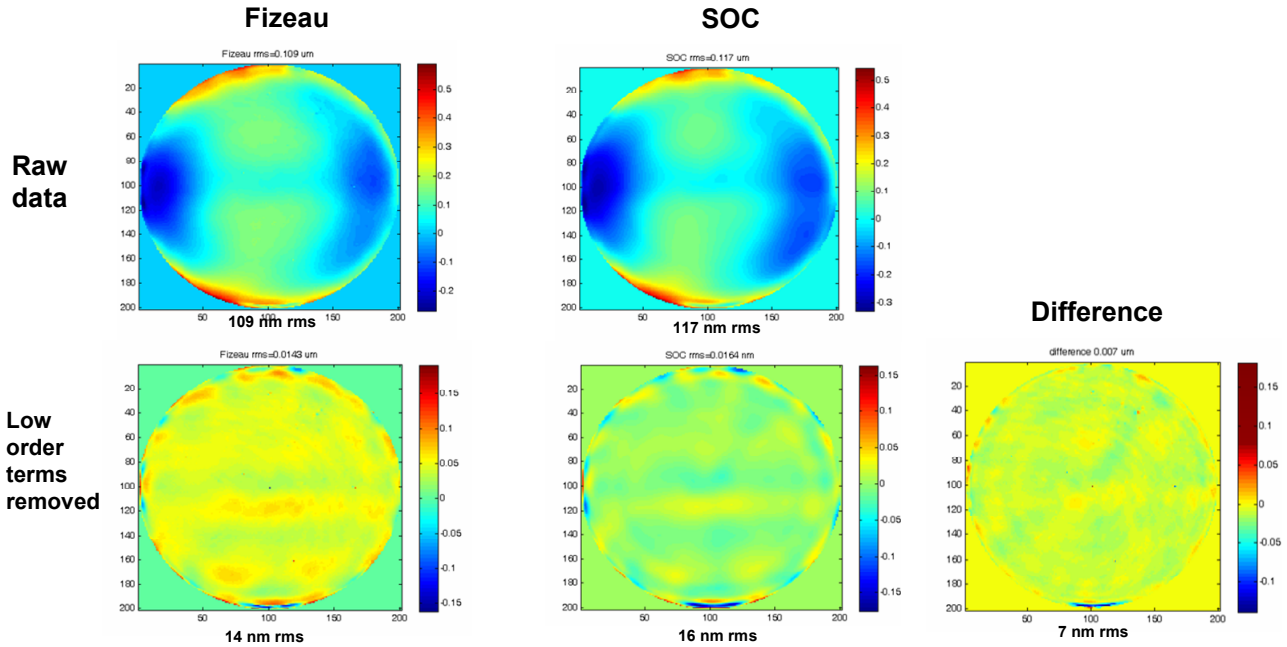

Figure 15. The measurements with the SOC and the Fizeau system show excellent agreement. After removing low order terms, the SOC is expected to be accurate to 6 nm rms and the Fizeau test was constructed to be accurate to 3 nm rms.

Two additional features of this test have recently been proven at the University of Arizona as part of a different program:

- Vibration insensitive simultaneous phase shift interferometry. The point source was replaced by a pair of fiber-fed source points with opposite circular polarization. The geometry is configured so one source will create the test wavefront and the reference wavefront is created by the other source.[8] Then the two wavefronts are combined and fed into a pixilated phase sensor from 4D Technologies[9]. This creates an array of pixels with 90° phase shift which is used to calculate the wavefront variations.
- Noise reduction with synthetic extended source. Coherent noise from ghost reflections and from dust on the optics is typically mitigated by using a spinning ground glass screen to average out the noise during an exposure. This is not possible with the dual source system, as it would cause the fringes themselves to wash out. So rather than average the noise during an exposure, we make multiple measurements and average the resulting maps. Since the vibration insensitive system captures data so quickly, it takes only a couple of minutes to capture data where all of the noise is reduced to a few nm rms.

6. CONCLUSION

The CGH Fizeau test was evaluated and shown to provide a viable method for measuring the E-ELT and TMT primary mirror segments. Some key advantages are:

- High accuracy for surface figure measurement, including radius of curvature matching
- Low noise measurements achieved by common path interferometry, which minimizes sensitivity to noise from air motion and vibration
- Test is fully calibrated with a reference sphere. Redundant tests made by rotating test plate and calibration sphere validate the error budget.
- Excellent efficiency is possible, requiring no calibration between segment measurements, only a change in holograms.

This method shows considerable promise for providing accurate and efficient measurements of the numerous segments required for these new large telescopes.

7. REFERENCES

1) J. Nelson and G. H. Sanders, "The status of the Thirty Meter Telescope project," Proc. SPIE **7012**, 70121A (2008).
2) R. Gilmozzi and J. Spyromilio, "The European Extremely Large Telescope (E-ELT)," Messenger **127**, 11-19(2007).
3) J. H. Burge, "Efficient testing of off-axis aspheres with test plates and computer-generated holograms," Proc. SPIE **3782**, 349–357 (1999).
4) F. Y. Pan and J. Burge, "Efficient Testing of Segmented Aspherical Mirrors by Use of Reference Plate and Computer-Generated Holograms. I. Theory and System Optimization," Appl. Opt. **43**, 5303-5312 (2004).
5) F. Y. Pan, J. Burge, D. Anderson, A. Poleshchuk, "Efficient Testing of Segmented Aspherical Mirrors by Use of a Reference Plate and Computer-Generated Holograms. II. Case Study, Error Analysis, and Experimental Validation," Appl. Opt. **43**, 5313-5322 (2004).
6) P. Su, J. H. Burge, and R. E. Parks, "Application of maximum likelihood reconstruction of subaperture data for measurement of large flat mirrors," Appl. Opt. **49**, 21-31 (2010).
7) J. H. Burge, *et al.*, "Fabrication and testing of 1.4-m convex off axis aspheric optical surfaces," Proc. SPIE **7426**, (2009).
8) M. B. Dubin, C. Zhao, J. H. Burge, "Fizeau interferometer with spherical reference and CGH correction for measuring of large convex aspheres," Proc. SPIE **7426**, (2009).
9 Millerd, J.E., Brock, N.J., Hayes, J.B., North-Morris, M.B., Novak, M., and Wyant, J.C., "Pixelated phase-mask dynamic interferometer," Proc. SPIE **5531,** 304-314, (2004).